POLITECNICO
MILANO 1863

RE.PUBLIC@POLIMI
Research Publications at Politecnico di Milano

Post-Print

This is the accepted version of:

Wang, Xiao; Xia, Pinqi
Novel Modeling and Vibration Analysis Method on a Helicopter Drive Train System
AIAA Journal, Vol. 60, N. 7, 2022, p. 4288-4301
doi: 10.2514/1.j061493

The final publication is available at https://doi.org/10.2514/1.j061493

Access to the published version may require subscription.

When citing this work, cite the original published paper.

Novel Modeling and Vibration Analysis Method on a Helicopter Drive Train System

Xiao Wang* and Pinqi Xia†
Nanjing University of Aeronautics and Astronautics, 210016 Nanjing, People's Republic of China

When it comes to analyzing the dynamic characteristics of a geared system, it is common practice to create an equivalent mathematical model for which the rotational velocity is the same for all the elements. In contrast to creating the equivalent system firstly, a novel strategy based on the transfer matrix method is developed, which can directly obtain the equation of motion according to the system topology figure. Actually, any kind of topology of the system, e.g., geared branch or geared closed-loop systems, can be decoupled into a combination of a series of independent chain systems via introducing the virtual branched-gear transfer matrix. The overall transfer equation of the system can be efficiently obtained because the transfer matrix method of a chain system is simply matrix multiplication. The transfer matrices of typical gear types, e.g., reduction gear and planetary gear, are derived. In particular, a simple and aesthetic transfer matrix of rotating beam is derived to solve the rotor blade flapping or lead-lag vibration problems. A dimension reduction strategy is also introduced to address the dimension unmatched issue, further reducing the scale of the overall transfer matrix of the system. At last, an application on modeling an analysis of the coupled flexible rotor blade/engine/tail rotor/drive train system of a helicopter is presented.

Nomenclature

EI	=	bending stiffness
$\boldsymbol{I}$	=	identity matrix
J	=	moment of inertia
J_p	=	polar moment of inertia
K	=	torsional stiffness of the shaft
k	=	torsional stiffness of the shaft
L	=	length of the blade
l	=	length of the shaft
M_z	=	bending moment about z-axis
m	=	mass of the element
m_0	=	mass per unit length
N_i	=	number of teeth of the i gear
n_p	=	number of planet gears in an epicyclic gear train
P	=	centrifugal force
Q_x, Q_y	=	shear force on x axis and y axis
R_i	=	radius of the i gear
r_H	=	radius of the hub
T	=	shaft torque
$\boldsymbol{U}$	=	transfer matrix
V	=	bending displacement of the beam
v	=	bending displacement
$\boldsymbol{z}$	=	state vector
Δ	=	determinate value
δ	=	variation operator
η	=	gear ratio
Θ	=	angular displacement
θ_i	=	angular displacement of i gear
ρ	=	mass density
Ω	=	rotational speed
ω	=	natural frequency
$\dot{()}$, $\ddot{()}$	=	$\partial()/\partial t$, $\partial^2()/\partial t^2$
$()'$, $()''$	=	$\partial()/\partial x$, $\partial^2()/\partial x^2$
Ⓢ	=	virtual geared branch element
Ⓖ	=	geometry element
Ⓓ	=	dimension reduction element

*Associate Professor, National Key Laboratory of Rotorcraft Aeromechanics, College of Aerospace Engineer, No. 29 Yudao Street, Jiangsu Province.

†Professor, National Key Laboratory of Rotorcraft Aeromechanics, College of Aerospace Engineer, No. 29 Yudao Street, Jiangsu Province.

I. Introduction

GEAR systems are widely used in many types of rotating machines, e.g., propulsive systems of marine engines and transmission systems of helicopters, for achieving different rotational speeds for some of the machine elements [1]. In addition to changing speed, the gear systems can also change the torque, and the direction of a power source. A typical helicopter transmission system transfers power from the engines to the main rotor, trail rotor, and other accessories. The primary job of the helicopter main gear box is to reduce engine output from high rotation speed to the optimum main rotor and tail rotor rotation speed [2]. Inadequate integration of the rotor, engine, transmission system, and the associated control system may induce several undesired consequences, e.g., excessive loads in the rotor or drive components, inadequate maneuvering performance, or unacceptable vehicle handling qualities [3–5]. Recently, Guglieri [6] gave a comprehensive discussion on the effect of drive train and fuel control design on helicopter handling qualities. Muscarello et al. [7] highlighted the interaction between the engine-drive train system and deformable rotorcraft airframes by considering the connections constraining the gearboxes to the airframe structure. Sidle et al. [8] investigated the coupled structural dynamic response of an elastic airframe and engines due to the main rotor hub load by using a fast computing substructuring approach. Rigo et al. [9] discussed drive train modeling effects on tiltrotor aeroelastic analysis. Weiss and Kessler [10] gave a load prediction of hingeless helicopter rotors when considering the drive train dynamics.

A typical flowchart of modeling and analysis of the geared shaft systems follows obtaining an equivalent system in which all the elements keep the same rotational speed, and then using the finite element method (FEM) to discretize the equivalent system [11–13]. In contrast to creating the equivalent system, a transfer matrix-based method is developed to directly obtain the system governing equation according to the system topology. The transfer matrix method was developed in the 20th century to addressing elastomechanical problems, exhibiting powerful computing efficiency [14–16]. Holzer [17] first used the transfer matrix method to address the torsional vibration problem of shafts with multiple discs. Myklestad [18] used a similar method applied to the modal analysis of helicopter blades. Rui and his coworkers extended the transfer matrix method to modeling and analyzing the multibody systems dynamics, also known as Rui's method [19–21]. Back in the long river of mechanics history, the

multibody system dynamics modeling technologies have been developed over the last 60 years. The main differences are essentially related to three aspects: the choice of variables, the treatment of kinematical constraints, and degree of reduction toward a minimal set of equations [22–24]. However, Rui's method provides a totally new approach to this problem based on the transfer matrix method. Highlights of Rui's method include no need for the global dynamics equation of the system, high programming, low order of matrix involved, and high efficiency. The modeling method developed in this paper build on top of Rui's method [20], preserving its advantages.

A new kind of virtual branched gear transfer matrix is introduced, which can decouple any kind of geared topology, e.g., geared branch topology or geared closed-loop topology, to a combination of a series of independent chain topologies. This can significantly further reduce the difficulty of geared system modeling, because the transfer matrix method of a chain system is simply matrix multiplication [25]. In fact, one can directly write the equation of motion of the geared system according to the topology figure of the system, which can be drawn as a sum of chain systems via the presented method. In addition, the transfer matrices of the typical gear types, e.g., reduction gear and planetary gear, are also derived. Note that, the transfer matrix solely needs to be solved once, after which it can be archived in a transfer matrix library as that offered in Ref. [20]. A dimension reduction strategy is also introduced to address the possible dimension unmatched issue, further reducing the order of the overall transfer matrix of the system.

An application on modeling an analysis of the coupled flexible rotor blade/engine/tail rotor/drive train system of a helicopter is presented. In particular, a simple and aesthetic transfer matrix of rotating beam is derived to solve the rotor blade flapping or lead-lag vibration problems. The fundamental characteristics of the coupled hingeless rotor and drive train dynamics of a typical helicopter are investigated, because a hingeless rotor is expected to be more influenced by the drive train due to direct moment transmission at the blade attachment [26]. Eigenanalysis results including frequencies and mode shapes are presented for the linearized system without the effect of rotor aerodynamics.

II. Modeling Strategy

Gears are widely used in different machines to change the speed, torque, and direction of a power source. From the perspective of the system topology figure, three typical types of geared system can be summarized: geared chain system, geared branched system, and geared closed-loop system.

It should be noted that the gears are considered kinematically and dynamically ideal here, meaning that the teeth compliance is neglected; phenomena like nonsmooth contact dynamics, the number of teeth simultaneously in contact, and the corresponding rattling and ripple are ignored; power losses due to friction and so on are not of concern in the present work. The geared system considered here is actually solely a one-dimensional system, the state vector of which can be normally defined as

$$z = [\Theta, T]^T \tag{1}$$

where Θ is the angular displacement, and T is the torque.

A. Geared Chain System

Before introducing the method for modeling the geared chain system, two typical gear mathematical models, i.e., simple gear model and planetary gear model, described based on the transfer matrix method are developed.

1. *Simple Gear Model*

A simplified simple gear mathematical model, which can be the model of spur gear, bevel gear, screw gear, etc. [1], is shown in Fig. 1. There are several methods to obtain the transfer matrix of the gear [20]. Here, a classical transfer matrix modeling strategy [14] is adopted. It is assumed that the moment of inertia of the input (master) gear is J_I and that of the output (slave) gear is J_O; thus the transfer matrix of the simple gear system is

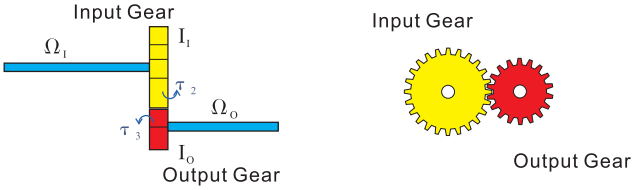

Fig. 1 Simple gear model.

$$\begin{aligned} \boldsymbol{U} &= \underbrace{\begin{bmatrix} 1 & 0 \\ -\omega^2 J_I & 1 \end{bmatrix}}_{\text{inputgear}} \underbrace{\begin{bmatrix} -\eta & 0 \\ 0 & -\frac{1}{\eta} \end{bmatrix}}_{\text{contact}} \underbrace{\begin{bmatrix} 1 & 0 \\ -\omega^2 J_O & 1 \end{bmatrix}}_{\text{outputgear}} \\ &= \begin{bmatrix} -\eta & 0 \\ \frac{J_I \omega^2}{\eta} + J_O \omega^2 \eta & -\frac{1}{\eta} \end{bmatrix} \end{aligned} \tag{2}$$

where ω is the frequency of the system, and η is the gear ratio, which can be defined as

$$\eta = \frac{N_I}{N_O} = \frac{\Omega_O}{\Omega_I} = \frac{R_I}{R_O} \tag{3}$$

where $N_{I,O}$, $\Omega_{I,O}$, and $R_{I,O}$ are the number of teeth, the rotational speed, and the radius of the associated gears, respectively. The subscripts I and O denote input gear and the output gear, respectively. The gear ratio will be described by the number of teeth of the gear unless otherwise stated in this paper.

2. *Planetary Gear or Epicyclic Gear*

An epicyclic gear train (planetary gear) consists of two gears mounted so that the center of one gear revolves around the center of the other [1]. As shown in Fig. 2, the basic components of the epicyclic gear include a sun gear (the center), planet gears (around the sun gear), a carrier (holds one or more peripheral planet gears), and a ring (an outer ring with inward-facing teeth that mesh with planet gears).

The analytical mechanics technique is used to obtain the transfer matrix of the planetary gear. Following Hamilton's principle [27], the governing equations of the planetary gear can be given as

$$\begin{aligned} &T_s \delta\theta_s + T_r \delta\theta_r + T_c \delta\theta_c \\ &= \left[J_s \ddot{\theta}_s + \frac{R_s^2}{R_p^2} n_p J_p \ddot{\theta}_s - \frac{(R_s + R_p) R_s}{R_p^2} n_p J_p \ddot{\theta}_c \right] \delta\theta_s + J_r \ddot{\theta}_r \delta\theta_r \\ &\quad + \left[J_c \ddot{\theta}_c + \left(\frac{R_s + R_p}{R_p} \right)^2 n_p J_p \ddot{\theta}_c - \frac{(R_s + R_p) R_s}{R_p^2} n_p J_p \ddot{\theta}_s \right. \\ &\quad \left. + (R_s + R_p)^2 n_p m_p \ddot{\theta}_c \right] \delta\theta_c \end{aligned} \tag{4}$$

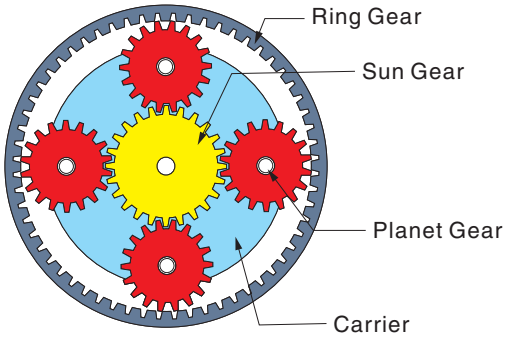

Fig. 2 Planetary gear model.

where n_p is the number of plant gears, and m_p is the mass of a single plant gear. $T_{s,r,c}$, $\theta_{s,r,c}$, $J_{s,p,r,c}$, and $R_{s,p,r,c}$ are the associated external torque, angular displacements, moments of inertia, and the geometry radius, respectively. The subscripts s, p, r, and c denote the sun gear, the planet gear, the ring gear, and the carrier, respectively.

In addition, according to the sun–planet and planet–ring interaction, it can be obtained

$$\dot{\theta}_c = \frac{N_s}{N_s + N_r}\dot{\theta}_s + \frac{N_r}{N_s + N_r}\dot{\theta}_r \tag{5}$$

where N_s and N_r are the number of teeth of the sun and that of the ring gear, respectively. If the ring gear is locked, i.e., $\dot{\theta}_r = 0$, the sun gear is the input gear, while the planet carrier is the output gear. The gear ratio can be obtained from Eq. (6):

$$\eta = \frac{N_s}{N_s + N_r} = \frac{N_s}{2(N_s + N_p)} \tag{6}$$

Thus, Eq. (4) can be simplified as

$$T_s + \frac{R_s}{2(R_s + R_p)}T_c = \underbrace{\left[\underbrace{J_s}_{\text{sun gear}} + \underbrace{n_p \frac{R_s^2}{4}\left(\frac{1}{R_p^2}J_p + m_p\right)}_{\text{planet gears}} + \underbrace{\left(\frac{R_s}{2(R_s + R_p)}\right)^2 J_c}_{\text{planet carrier}}\right]}_{\text{Effective inertia of the epicyclic gear}}\ddot{\theta}_s \tag{7}$$

The state vector of the torsional system is defined as

$$z_{\text{out}} = \Theta_{\text{out}} T_{\text{out}} = \eta\Theta_{\text{in}}\frac{1}{\eta}T_{\text{in}} - \frac{1}{\eta}J_e\omega^2\Theta_{\text{in}} = \begin{bmatrix} \eta & 0 \\ -\frac{1}{\eta}\omega^2 J_e & \frac{1}{\eta} \end{bmatrix}\begin{Bmatrix} \Theta_{\text{in}} \\ T_{\text{in}} \end{Bmatrix} \tag{8}$$

where the effective inertia of the epicyclic gear J_e is defined as

$$J_e = J_s + n_p \frac{R_s^2}{4}\left(\frac{1}{R_p^2}J_p + m_p\right) + \eta^2 J_c \tag{9}$$

Thus, the transfer matrix of a planetary gear with locked ring gear can be given as

$$\boldsymbol{U} = \begin{bmatrix} \eta & 0 \\ -\frac{1}{\eta}\omega^2 J_e & \frac{1}{\eta} \end{bmatrix} \tag{10}$$

3. Geared Chain System

A typical geared chain system with one simple gear that is used to adjust the rotational speed of the two mounted shafts is shown in Fig. 3a, of which the topology figure is drawn in Fig. 3b. In Fig. 3b, the circle denotes the elements, and the arrow denotes the transfer direction. Specifically, circles 1, 2, 3, 4, and 5 are disk4, shaft2, gears, shaft 1, and disk 1, respectively. Long-winded again, the arrows in the topology figure only denote the matrix transfer direction; all the elements, including rigid bodies, hinges, and flexible beams, are represented in circles.

The transfer matrix of the rigid disk and the flexible shaft have been given in the transfer matrix library of Ref. [20].

The transfer matrix of the rigid disk is

$$\boldsymbol{U} = \begin{bmatrix} 1 & 0 \\ -\omega^2 J & 1 \end{bmatrix} \tag{11}$$

where J is moment of inertia of the disk, and ω is the frequency of the system.

The free torsional vibration equation of the elastic shaft is

$$K\frac{\partial^2\theta_x}{\partial x^2} - \rho J_p \frac{\partial^2\theta_x}{\partial t^2} = 0 \tag{12}$$

where θ_x is the rotational angle, ρ is the mass density of the shaft, J_p is the polar moment of inertia, and K is the torsional stiffness of the shaft. Taking $\theta_x(x, t) = \Theta(x)e^{i\omega t}$ into Eq. (12) yields

$$\frac{\partial^2\Theta}{\partial x^2} + \omega^2\frac{\rho J_p}{K}\Theta = 0 \tag{13}$$

The general solution of Eq. (13) can be given as

$$\Theta = A_1 \sin\gamma x + A_2 \cos\gamma x \tag{14}$$

where $\gamma^2 = \omega^2(\rho J_p/K)$, A_1, and A_2 are arbitrary constants. According to the definition of the torque $T = K(\mathrm{d}\Theta/\mathrm{d}x)$ in the Mechanics of Materials [28], the state vector of the shaft at an arbitrary point x can be obtained as

$$\begin{Bmatrix} \Theta(x) \\ T(x) \end{Bmatrix} = \begin{bmatrix} \sin\gamma x & \cos\gamma x \\ \gamma K\cos\gamma x & -\gamma K\sin\gamma x \end{bmatrix}\begin{Bmatrix} A_1 \\ A_2 \end{Bmatrix} \tag{15}$$

The transfer equation of the elastic shaft with length l from input end $x = 0$ to the output end $x = l$ then can be obtained:

$$\begin{Bmatrix} \Theta \\ T \end{Bmatrix}_{\text{output}} = \begin{bmatrix} \cos\gamma l & \frac{\sin\gamma l}{\gamma K} \\ -\gamma K\sin\gamma l & \cos\gamma l \end{bmatrix}\begin{Bmatrix} \Theta \\ T \end{Bmatrix}_{\text{input}} \tag{16}$$

Thus, the transfer matrix of the elastic shaft with uniform cross section is

$$\boldsymbol{U} = \begin{bmatrix} \cos\gamma l & \frac{\sin\gamma l}{\gamma K} \\ -\gamma K\sin\gamma l & \cos\gamma l \end{bmatrix} \tag{17}$$

If the shaft is considered massless, the transfer matrix (17) will be reduced as

$$\boldsymbol{U} = \begin{bmatrix} 1 & \frac{l}{K} \\ 0 & 1 \end{bmatrix} \tag{18}$$

The equation of motion of the chain system of Fig. 3 described in transfer matrix way is

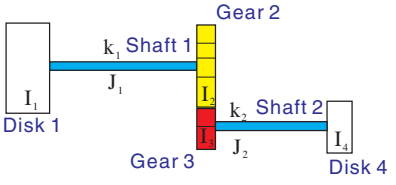

a) A typical gear chain system

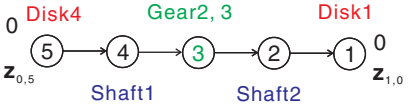

b) Topology figure of the gear chain system

Fig. 3 Topology figure of the gear chain system in transfer matrix method.

$$\underbrace{\boldsymbol{U}_1}_{\text{Eq.(11)}}\underbrace{\boldsymbol{U}_2}_{\text{Eq.(17)}}\underbrace{\boldsymbol{U}_3}_{\text{Eq.(2)}}\underbrace{\boldsymbol{U}_4}_{\text{Eq.(17)}}\underbrace{\boldsymbol{U}_5}_{\text{Eq.(11)}} z_{0,5} = z_{1,0} \tag{19}$$

Moving the right terms to the left, it can be written as

$$\begin{bmatrix} \boldsymbol{U}_1\boldsymbol{U}_2\boldsymbol{U}_3\boldsymbol{U}_4\boldsymbol{U}_5 & -\boldsymbol{I} \end{bmatrix} \begin{Bmatrix} z_{0,5} \\ z_{1,0} \end{Bmatrix} = \boldsymbol{0} \tag{20}$$

Note that Eq. (20) gives the general form of the equation of motion modeling with the transfer matrix method. It can be found that the equation of motion can be directly obtained by introducing the transfer matrix of the gear, no more need to create the equivalent system.

B. Geared Branch System (Tree System)

A typical geared branch system as shown in Fig. 4a is discussed. The transmission gear box, which is marked with a dashed rectangle in Fig. 4a, is treated as a single element; thus the related topology figure can be drawn as shown in Fig. 4b. The transfer directions and the meanings of each elements have also been indicated in Fig. 4b. A agreement is made that only one boundary end is considered as the root, of which the state vector is normally given as $z_{1,0}$; whereas the others are all considered as the tips, of which the state vectors are denoted as $z_{0,j}$, where j is the sequence number of the tip element.

Considering the fact that the overall transfer matrix of the chain system is simply matrix multiplication as discussed in Sec. II.A, it will greatly reduce the difficulty of modeling if the geared branch system can be redescribed as a collection of multiple chain systems. To achieve this target, a virtual geared branch element Ⓢ is defined:

$$\boldsymbol{U}_S = \begin{bmatrix} 0 & 0 \\ \frac{1}{\eta}\omega^2 J_I & -\frac{1}{\eta} \end{bmatrix} \tag{21}$$

where η is the gear ratio, and J_I is the moment of inertia of the input gear. When introducing the virtual geared branch element into the system, the geared branch system is split into two independent chain systems as shown in Fig. 5.

Then the governing equation can be given as the sum of the two chains:

$$\begin{bmatrix} \underbrace{\boldsymbol{U}_1\boldsymbol{U}_2\boldsymbol{U}_S\boldsymbol{U}_6\boldsymbol{U}_7}_{\boldsymbol{U}_{c1}} & \underbrace{\boldsymbol{U}_1\boldsymbol{U}_2\boldsymbol{U}_3\boldsymbol{U}_4\boldsymbol{U}_5}_{\boldsymbol{U}_{c2}} & -\boldsymbol{I} \end{bmatrix} \begin{Bmatrix} z_{0,7} \\ z_{0,5} \\ z_{1,0} \end{Bmatrix} = \boldsymbol{0} \tag{22}$$

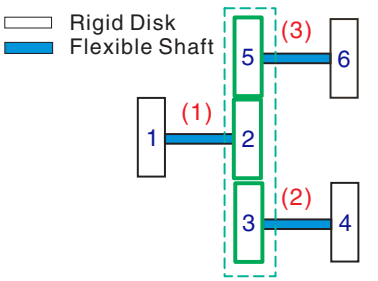

a) A typical gear-branched system

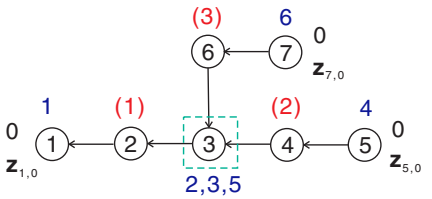

b) Topology figure

Fig. 4 Topology figure of the gear-branched system in transfer matrix method.

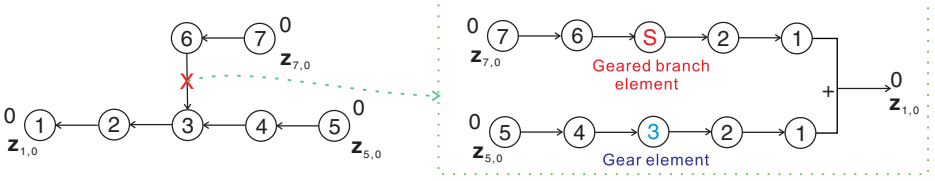

Fig. 5 Geared branch system split into independent chain systems.

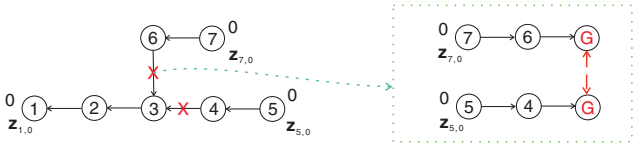

Fig. 6 Additional geometrical constraints of the geared branch system.

where the expressions of $(\boldsymbol{U}_1\boldsymbol{U}_5\boldsymbol{U}_7)$, $\boldsymbol{U}_3$, and $(\boldsymbol{U}_2\boldsymbol{U}_4\boldsymbol{U}_6)$ are given in Eqs. (11), (2), and (17), respectively. One may notice that the number of unknown variables in Eq. (22) is more than that of algebraic equations. Therefore, additional constraints should be involved. The additional constraint is that the geometry boundaries at the branched point from the different input ends should be equaled. Figure 6 depicts this geometrical constraint by introducing the virtual gear geometry elements Ⓖ, of which the transfer matrix is defined as

$$\boldsymbol{U}_G = \begin{bmatrix} -\eta & 0 \end{bmatrix} \tag{23}$$

where η is the associated gear ratio. In fact, the function of the virtual gear geometry element is to extract the geometric information of the state vector, because the torque information has been transferred by the geared branch element of Eq. (21). The equation of the additional constraints then can be given as

$$\underbrace{\boldsymbol{U}_G\boldsymbol{U}_6\boldsymbol{U}_7 z_{0,7}}_{\boldsymbol{U}_{g1}} = \underbrace{\boldsymbol{U}_G\boldsymbol{U}_4\boldsymbol{U}_5 z_{0,5}}_{\boldsymbol{U}_{g2}} \tag{24}$$

Combining the governing Eq. (22) and the geometry constraint (24), the overall equation of motion of the system as given in Fig. 4a is

$$\begin{bmatrix} \boldsymbol{U}_{c1} & \boldsymbol{U}_{c2} & -\boldsymbol{I} \\ \boldsymbol{U}_{g1} & -\boldsymbol{U}_{g2} & \boldsymbol{0} \end{bmatrix} \begin{Bmatrix} z_{0,7} \\ z_{0,5} \\ z_{1,0} \end{Bmatrix} = \boldsymbol{0} \tag{25}$$

A drawn strategy of the topology figure for a geared branch system is concluded as shown in Fig. 7. One can directly write the overall equation of motion of the system according to its topology figure; see Eq. (25). In conclusion, $N-1$ virtual geared branch elements Ⓢ and $N-1$ virtual gear geometry elements Ⓖ should be introduced into the N branched tree system, and then the overall equations can be written as the sum of N independent chain systems with $N-1$ geometrical constraints, e.g.,

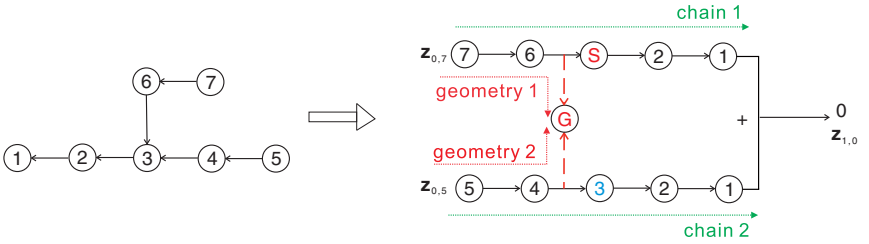

Fig. 7 A typical topology figure of the geared branch system.

$$\begin{bmatrix} \boldsymbol{U}_{c1} & \boldsymbol{U}_{c2} & \cdots & \cdots & \boldsymbol{U}_{cN} & -\boldsymbol{I} \\ \boldsymbol{U}_{g1} & -\boldsymbol{U}_{g2} & \boldsymbol{0} & \cdots & \cdots & \boldsymbol{0} \\ \boldsymbol{0} & \boldsymbol{U}_{g2} & -\boldsymbol{U}_{g3} & \cdots & \cdots & \boldsymbol{0} \\ \vdots & \vdots & \vdots & \vdots & \vdots & \vdots \\ \boldsymbol{0} & \boldsymbol{0} & \boldsymbol{0} & \boldsymbol{U}_{g(N-1)} & -\boldsymbol{U}_{gN} & \boldsymbol{0} \end{bmatrix} \begin{Bmatrix} z_{0,c1} \\ z_{0,c2} \\ \vdots \\ z_{0,cN} \\ z_{1,0} \end{Bmatrix} = \boldsymbol{0} \tag{26}$$

$$\begin{bmatrix} \underbrace{\boldsymbol{U}_1\boldsymbol{U}_S\boldsymbol{U}_5}_{\text{chain1}} & \underbrace{\boldsymbol{U}_1\boldsymbol{U}_2\boldsymbol{U}_3\boldsymbol{U}_4}_{\text{chain2}} & -\boldsymbol{I} \\ \underbrace{\boldsymbol{U}_G\boldsymbol{U}_5}_{\text{geometry1}} & \underbrace{\boldsymbol{U}_G\boldsymbol{U}_3\boldsymbol{U}_4}_{\text{geometry2}} & \boldsymbol{0} \\ \boldsymbol{0} & \boldsymbol{0} & \underbrace{\boldsymbol{U}_1\boldsymbol{U}_2\boldsymbol{U}_3 - \boldsymbol{I}}_{\text{constraint}} \end{bmatrix} \begin{Bmatrix} z_{0,5} \\ z_{0,4} \\ z_{1,0} \end{Bmatrix} = \boldsymbol{0} \tag{29}$$

C. Geared Closed-Loop System

The topology figure of a simplest closed-loop system is presented in Fig. 8. After cutting the junction of any two adjacent elements, e.g., elements 1 and 3, the system can be represented as a single chain system with a constraint. The constraint can be represented as that the boundary ends at the cutting point have the same state vectors.

$$\begin{cases} \text{chain: } z_{1,0} = \boldsymbol{U}_1\boldsymbol{U}_2\boldsymbol{U}_3 z_{0,3} \\ \text{constraint: } z_{1,0} = z_{0,3} \end{cases} \tag{27}$$

Thus the overall equation of motion for a closed-loop system is

$$[\boldsymbol{U}_1\boldsymbol{U}_2\boldsymbol{U}_3 - \boldsymbol{I}]z_{1,0} = \boldsymbol{0} \tag{28}$$

To further make a deeper understanding of the presented modeling strategy, the topology figure of a geared branch system with a closed-loop can be drawn as shown in Fig. 9. Following the steps introduced previously, each chain is filled in the corresponding column of the first row of the overall transfer matrix, and each constraint is written in a separate row. Thus, the equation of motion of Fig. 9 can be directly written as

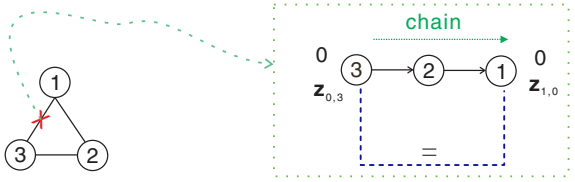

Fig. 8 A typical topology figure of the geared closed-loop system.

III. Modeling of the Coupled Rotor Blades/Engine/Drive Train System

Figure 10 depicts a schematic of the helicopter drive train, in which a simplified main gear box configuration is highlighted. The main rotor blades are considered as flexible beams, whereas the tail rotor is considered as a rigid disk. The coupled flexible rotor blades/engine/drive train system as shown in Fig. 10 can also be presented with circles (elements) and arrows (directions) as shown in Fig. 11. The meaning of each element that has been indicated in Fig. 10 is given in Table 1.

The explicit expressions of the transfer matrix of each element in Table 1 have been included in the library of Ref. [20], except the rotating beam element. Although a transfer matrix of a rotating Euler–Bernoulli beam is derived by using the Frobenius method [29] in Ref. [30], the associated expression is too sophisticated to give a specific expression directly. Moreover, the transfer matrix of Ref. [20] can only deal with out-of-plane (flapping) vibration but not horizontal (lead-lag) vibration. Thus, a simpler and more aesthetic transfer matrix of rotating beam is derived to treat both the flapping and lead-lag vibrations. Note that the transfer matrix of the rotating beam is a numerical approximate solution, because there is no analytical solution.

Before drawing the topology figure with the method proposed in Sec. II, there are two more issues that should be discussed firstly, i.e., the transfer matrix of the flexible rotating blade and the dimensions unmatched issue between the rotor blade and the rigid hub.

A. Transfer Matrix of the Flexible Rotating Blade

The flexible rotor blade can be modeled as a rotating beam when only the structural dynamic characteristics are investigated. The linearized free vibration equation of a rotating beam in lead-lag motion can be expressed as [31]

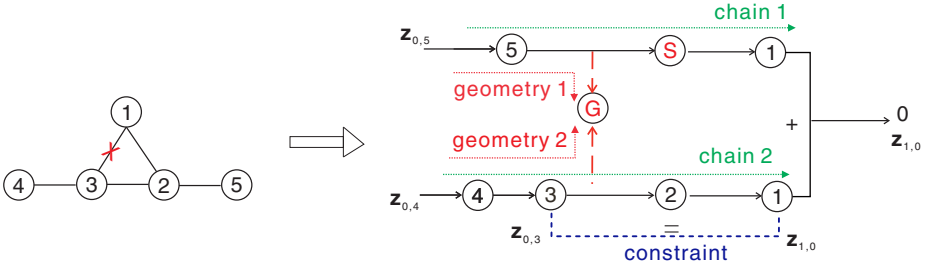

Fig. 9 A typical topology figure of the geared closed-loop system.

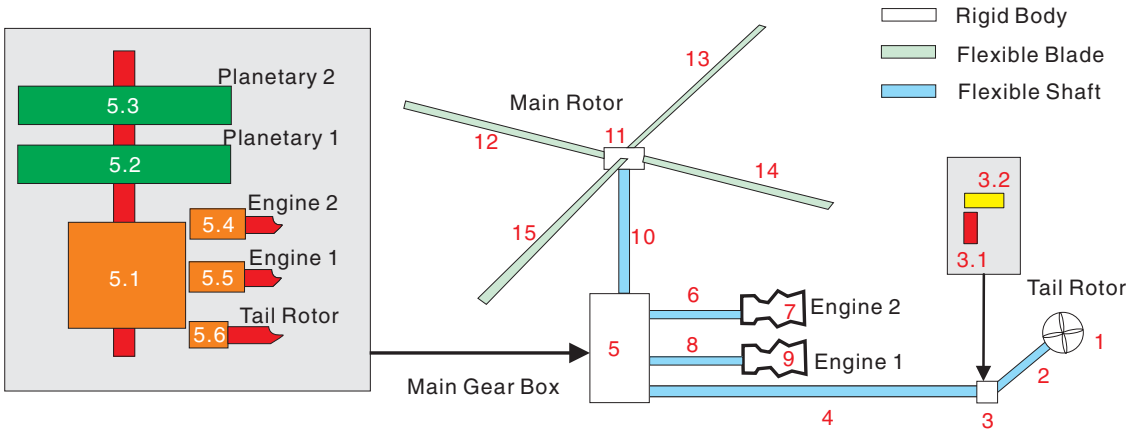

Fig. 10 A schematic of the helicopter drive train.

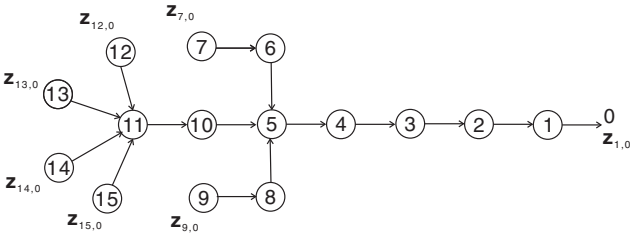

Fig. 11 Topology figure of the helicopter in Fig. 10.

Table 1 Meaning of the elements in topology figure presented in Fig. 11

No.	Meaning	Element type	Transfer matrix
1	Tail rotor	Rigid disk element	Eq. (11)
2, 4, 6, 8, 10	Transmission shaft	Massless shaft element	Eq. (18)
3, 5	Tail gear box, and main gear box	Gear element	Eqs. (2), (23), (10), (21)
7, 9	Engine	Rigid disk element	Eq. (11)
12, 13, 14, 15	Rotor blade	Flexible rotation beam element	Eq. (36)

$$\frac{\partial}{\partial x^2}\left[EI(x)\frac{\partial^2 V}{\partial x^2}\right]-\frac{\partial}{\partial x}\left[P(x)\frac{\partial V}{\partial x}\right]-\Omega^2 m_0(x)V+m_0(x)\frac{\partial^2 V}{\partial t^2}=0 \tag{30}$$

where $EI(x)$ is the bending stiffness, $m_0(x)$ is the mass per unit length, and the centrifugal force $P(x)$ is given as

$$P(x)=\int_x^L m_0(x)\Omega^2(r_H+x)\,\mathrm{d}x \tag{31}$$

where Ω, r_H, and L are the constant angular velocity, the radius of the hub, and the length of the blade, respectively. There is no analytical solution of Eq. (30), because the tension $P(x)$ depends on the spanwise station x, and thus the resulting equation is linear partial-differential and space-dependent. To model it with the transfer matrix method, the blade as shown in Fig. 12 is discretized into n beam elements each with a constant cross section. The bending stiffness

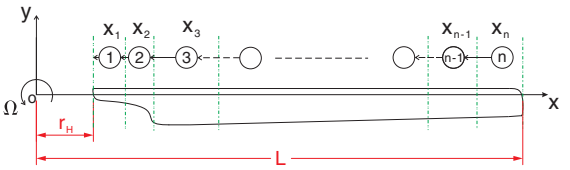

Fig. 12 A schematic of the rotating rotor blade.

and the mass per unit length of each element are considered as constants. Furthermore, it is assumed that the tension $P(x)$ resulting from the centrifugal force is also constant within each beam element. Note that the piecewise constant value of $P(x)$ is chosen at its midpoint here. Thus, assuming variable separation and an exponential time dependence $V(x,t)=v(x)e^{i\omega t}$ into Eq. (30) with the above assumptions, Eq. (30) will be transformed as a fourth-order differential equation:

$$EIv''''-Pv''-\Omega^2 m_0 v-\omega^2 m_0 v=0 \tag{32}$$

Solution of Eq. (32) can be expressed as

$$v(x)=C_1\cosh s_1x+C_2\sinh s_1x+C_3\cos s_2x+C_4\sin s_2x \tag{33}$$

where s_1 and s_2 are defined as

$$s_1=\sqrt{\frac{\sqrt{P^2+4(\omega^2+\Omega^2)m_0EI}}{2EI}+P},$$
$$s_2=\sqrt{\frac{\sqrt{P^2+4(\omega^2+\Omega^2)m_0EI}}{2EI}-P} \tag{34}$$

The state vector of an Euler–Bernoulli beam vibrating in-plane is

$$z=[v,\theta_z,M_z,Q_x]^T \tag{35}$$

where θ_z, M_z, and Q_x are the slop of the beam, the bending moment, and the shear force, respectively. Following the steps as introduced in the Appendix of Ref. [30], the transfer matrix of an uniform rotating beam element with length l can be obtained:

$$\boldsymbol{U}=\begin{bmatrix}
\frac{s_1^2\cos ls_2+s_2^2\cosh ls_1}{s_1^2+s_2^2} & \frac{\Gamma_1\sinh ls_1+\Gamma_2\sin ls_2}{\Lambda} & \frac{\cosh ls_1-\cos ls_2}{EI(s_1^2+s_2^2)} & \frac{s_1s_2(s_2\sinh ls_1-s_1\sin ls_2)}{\Lambda}\\
\frac{s_1s_2(s_2\sinh ls_1-s_1\sin ls_2)}{s_1^2+s_2^2} & \frac{s_1\Gamma_1\cosh ls_1+s_2\Gamma_2\cos ls_2}{\Lambda} & \frac{s_2\sin ls_2+s_1\sinh ls_1}{EI(s_1^2+s_2^2)} & \frac{s_1^2s_2^2(\cosh ls_1-\cos ls_2)}{\Lambda}\\
\frac{EIs_1^2s_2^2(\cosh ls_1-\cos ls_2)}{s_1^2+s_2^2} & \frac{EI(s_1^2\Gamma_1\sinh ls_1-s_2^2\Gamma_2\sin ls_2)}{\Lambda} & \frac{s_2^2\cos ls_2+s_1^2\cosh ls_1}{s_1^2+s_2^2} & \frac{EIs_1^2s_2^2(s_2\sin ls_2+s_1\sinh ls_1)}{\Lambda}\\
\frac{s_1^2\Gamma_1\sin ls_2+s_2^2\Gamma_2\sinh ls_1}{s_1s_2(s_1^2+s_2^2)} & \frac{\Gamma_1\Gamma_2(\cosh ls_1-\cos ls_2)}{s_1s_2\Lambda} & \frac{\Gamma_2\sinh ls_1-\Gamma_1\sin ls_2}{s_1s_2EI(s_1^2+s_2^2)} & \frac{s_1\Gamma_1\cos ls_2+s_2\Gamma_2\cosh ls_2}{\Lambda}
\end{bmatrix} \tag{36}$$

where P is the centrifugal force of the input end, while Γ_1, Γ_2, and Λ are defined as

$$\Gamma_1 = EIs_1s_2^4 + Ps_1s_2^2 + \Omega^2 m_0 s_1 \tag{37a}$$

$$\Gamma_2 = EIs_2s_1^4 - Ps_2s_1^2 + \Omega^2 m_0 s_2 \tag{37b}$$

$$\Lambda = EIs_1^4s_2^2 + EIs_1^2s_2^4 + \Omega^2 m_0 s_1^2 + \Omega^2 m_0 s_2^2 \tag{37c}$$

Note that the transfer matrix of Eq. (36) can also be used to describe the flapping motion of the blade when making $\Omega^2 m_0 = 0$, i.e., making

$$\Gamma_1 = EIs_1s_2^4 + Ps_1s_2^2 \tag{38a}$$

$$\Gamma_2 = EIs_2s_1^4 - Ps_2s_1^2 \tag{38b}$$

$$\Lambda = EIs_1^4s_2^2 + EIs_1^2s_2^4 \tag{38c}$$

$$s_1 = \sqrt{\frac{\sqrt{P^2 + 4\omega^2 m_0 EI}}{2\,EI} + P}, \quad s_2 = \sqrt{\frac{\sqrt{P^2 + 4\omega^2 m_0 EI}}{2\,EI} - P} \tag{38d}$$

This treatment is equivalent to eliminating the $\Omega^2 m_0 v$ term in Eq. (32), which then will be the equation of motion of the beam flapping motion.

Thus, the transfer matrix of the rotor blade that is discretized into n beam elements as presented in Fig. 12 is

$$\boldsymbol{U}_{\text{blade}} = \boldsymbol{U}_1\boldsymbol{U}_2 \cdots \boldsymbol{U}_{n-1}\boldsymbol{U}_n \tag{39}$$

There is no doubt that more elements taken into account may obtain better accuracy, because the centrifugal force is assumed to be constant, whereas it actually varies along the length. The influence of element number n will be discussed in Sec. IV.B.2.

B. Dimension Reduction Element

Comparing the state vectors of the rotor blade Eq. (35) and the rigid hub Eq. (1), it can be found that the dimensions of state vectors are not consistent. One can extend the state vector of the lower-dimensional element to match that of the highest-dimensional element to address this issue. However, this treatment will no doubt increase the scale of the overall transfer matrix of the system, and consume the unnecessary computing resources. Thus, a dimension reduction element Ⓓ is introduced to eliminate the unnecessary information. In other words, in contrast to the regular treatment [32], the state vector of the higher-dimensional element is artificially reduced to match that of the lowest one.

Figure 13 depicts a hub system with one blade, which also presents the associated topology figure when introducing the dimension reduction element. The hub can be considered as a rigid disk with radius r_H, of which the transfer matrix can be presented as

$$\begin{aligned}\boldsymbol{U}_2 &= \boldsymbol{U}_{2.1}\boldsymbol{U}_D\boldsymbol{U}_{2.2} \\ &= \underbrace{\begin{bmatrix} 1 & 0 \\ -\omega^2 J & 1 \end{bmatrix}}_{\text{Rigid disk(11)}} \underbrace{\begin{bmatrix} 0 & 1 & 0 & 0 \\ 0 & 0 & 1 & 0 \end{bmatrix}}_{\text{Dimension reduction element}} \underbrace{\begin{bmatrix} 1 & r_H & 0 & 0 \\ 0 & 1 & 0 & 0 \\ 0 & 0 & 1 & r_H \\ 0 & 0 & 0 & 1 \end{bmatrix}}_{\text{Massless rigid disk}} \\ &= \begin{bmatrix} 0 & 1 & 0 & 0 \\ 0 & -\omega^2 J & 1 & r_H \end{bmatrix}\end{aligned} \tag{40}$$

As shown in Eq. (40) and in Fig. 13, the hub is equivalent to two independent element, i.e., a rigid disk element at the center of the hub and a massless rigid disk with radius r_H. Once introducing the dimension reduction element, additional constraints should also be considered to explain the reason why the redundant dimensions can be eliminated. Thus, additional chains should be accounted. For example, the state vector from the blade to the hub, the information $[Y\ Q_x]$ should be eliminated, of which the reason is that there is no plane displacement of the hub:

$$\boldsymbol{U}_{DC}\boldsymbol{U}_3\boldsymbol{z}_{0,3} = \boldsymbol{0} \tag{41}$$

where the dimension-reduction-induced constraint element is defined as

$$\boldsymbol{U}_{DC} = [1 \quad 0 \quad 0 \quad 0] \tag{42}$$

The topology figure of the simple one blade hub system is drawn in Fig. 13, of which the one chain system is split into two independent two chains system. Thus, the equation of motion can be directly written as

$$\begin{bmatrix} \boldsymbol{U}_1\boldsymbol{U}_D\boldsymbol{U}_2\boldsymbol{U}_3 & -\boldsymbol{I} \\ \boldsymbol{U}_{DC}\boldsymbol{U}_3 & \boldsymbol{0} \end{bmatrix} \begin{Bmatrix} \boldsymbol{z}_{0,3} \\ \boldsymbol{z}_{1,0} \end{Bmatrix} = \boldsymbol{0} \tag{43}$$

C. Topology Figure of the Coupled Drive Train System

Introducing the virtual geared branch elements and the dimension reduction elements, the topology figure of the coupled rotor blades/engine/drive train system as shown in Fig. 10 then can be drawn as shown in Fig. 14. It can be seen that the system is decoupled into six independent chain systems accompanied with five geometry constraints, in combination with an additional constraint induced by dimension reduction. Thus, the equation of motion of the system can be written as

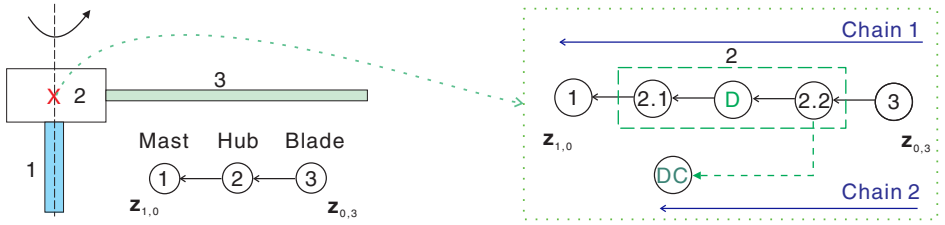

Fig. 13 The hub system with one blade.

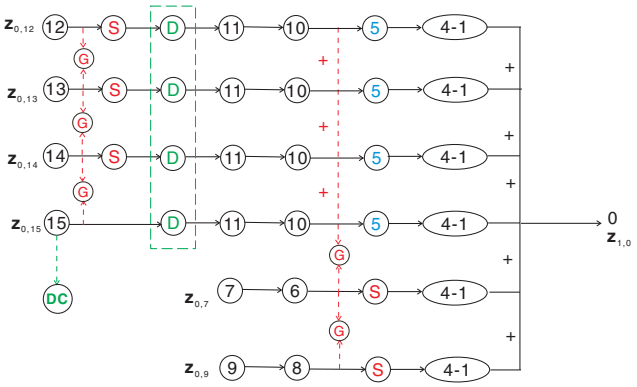

Fig. 14 Topology figure of the coupled rotor blades/engine/drive train system of Fig. 10.

IV. Results and Discussion

A. Eigenvalue Solution

The general equation of motion of a linear multibody system, e.g., Eq. (44), can be described as

$$\boldsymbol{U}_{\text{all}}\boldsymbol{z}_{\text{all}} = \boldsymbol{0} \tag{46}$$

Taking into account the boundary conditions in Eq. (46), it is normally either an essential (kinematic) boundary condition or a natural (force) boundary condition, and keeping the unknown state variables only, then Eq. (46) will be reduced as

$$\bar{\boldsymbol{U}}\,\bar{\boldsymbol{z}} = \boldsymbol{0} \tag{47}$$

$$\begin{bmatrix} \boldsymbol{U}_{c1} & \boldsymbol{U}_{c2} & \boldsymbol{U}_{c3} & \boldsymbol{U}_{c4} & \boldsymbol{U}_{c5} & \boldsymbol{U}_{c6} & -\boldsymbol{I} \\ \boldsymbol{U}_G\boldsymbol{U}_{12} & -\boldsymbol{U}_G\boldsymbol{U}_{13} & \boldsymbol{0} & \boldsymbol{0} & \boldsymbol{0} & \boldsymbol{0} & \boldsymbol{0} \\ \boldsymbol{0} & \boldsymbol{U}_G\boldsymbol{U}_{13} & -\boldsymbol{U}_G\boldsymbol{U}_{14} & \boldsymbol{0} & \boldsymbol{0} & \boldsymbol{0} & \boldsymbol{0} \\ \boldsymbol{0} & \boldsymbol{0} & \boldsymbol{U}_G\boldsymbol{U}_{14} & -\boldsymbol{U}_G\boldsymbol{U}_{15} & \boldsymbol{0} & \boldsymbol{0} & \boldsymbol{0} \\ \boldsymbol{U}_{g1} & \boldsymbol{U}_{g1} & \boldsymbol{U}_{g1} & \boldsymbol{U}_{g2} & -\boldsymbol{U}_{g3} & \boldsymbol{0} & \boldsymbol{0} \\ \boldsymbol{0} & \boldsymbol{0} & \boldsymbol{0} & \boldsymbol{0} & \boldsymbol{U}_{g3} & -\boldsymbol{U}_{g3} & \boldsymbol{0} \\ \boldsymbol{0} & \boldsymbol{0} & \boldsymbol{0} & \boldsymbol{0} & \boldsymbol{0} & \boldsymbol{U}_{DC}\boldsymbol{U}_{15} & \boldsymbol{0} \end{bmatrix} \begin{Bmatrix} z_{0,12} \\ z_{0,13} \\ z_{0,14} \\ z_{0,15} \\ z_{0,7} \\ z_{0,9} \\ z_{1,0} \end{Bmatrix} = \boldsymbol{0} \tag{44}$$

where the first row is the sum of the six chain systems, the second to sixth rows are the associated five geometry constraints, and the last (seventh) row is the constraint to the dimension reduction element. The explicit expressions of the transfer matrices in Eq. (44) are as follows:

$$\begin{aligned} \boldsymbol{U}_{c1} &= \boldsymbol{U}_{c2} = \boldsymbol{U}_{c3} = \boldsymbol{U}_1\boldsymbol{U}_2\boldsymbol{U}_3\boldsymbol{U}_4\boldsymbol{U}_5\boldsymbol{U}_{10}\boldsymbol{U}_{11}\boldsymbol{U}_D\boldsymbol{U}_F\boldsymbol{U}_{12}, \\ \boldsymbol{U}_{c4} &= \boldsymbol{U}_1\boldsymbol{U}_2\boldsymbol{U}_3\boldsymbol{U}_4\boldsymbol{U}_5\boldsymbol{U}_{10}\boldsymbol{U}_{11}\boldsymbol{U}_D\boldsymbol{U}_{12}, \\ \boldsymbol{U}_{c5} &= \boldsymbol{U}_{c6} = \boldsymbol{U}_1\boldsymbol{U}_2\boldsymbol{U}_3\boldsymbol{U}_4\boldsymbol{U}_S\boldsymbol{U}_8\boldsymbol{U}_9, \\ \boldsymbol{U}_{g1} &= \boldsymbol{U}_G\boldsymbol{U}_{10}\boldsymbol{U}_{11}\boldsymbol{U}_D\boldsymbol{U}_F\boldsymbol{U}_{12}, \\ \boldsymbol{U}_{g2} &= \boldsymbol{U}_G\boldsymbol{U}_{10}\boldsymbol{U}_{11}\boldsymbol{U}_D\boldsymbol{U}_{12}, \\ \boldsymbol{U}_{g3} &= \boldsymbol{U}_G\boldsymbol{U}_6\boldsymbol{U}_7 \end{aligned} \tag{45}$$

Actually, half of the state variables are zero due to the constraints for common boundary conditions. Making the typical gear-branched system as shown in Fig. 4 as an example, $\boldsymbol{z}_{\text{all}} = [\Theta_{0,7}\ \ T_{0,7}\ \ \Theta_{0,5}\ \ T_{0,5}\ \ \Theta_{1,0}\ \ T_{1,0}]^T$ is a 1×6 vector, and $\boldsymbol{U}_{\text{all}}$ is a 3×6 matrix as shown in Eq. (25). Taking into the free vibration boundaries, $\boldsymbol{z}_{\text{all}}$ will be reduced as a 1×3 vector, i.e., $\bar{\boldsymbol{z}} = [\Theta_{0,7}\ \ \Theta_{0,5}\ \ \Theta_{1,0}]^T$. Only keeping the associated columns in $\boldsymbol{U}_{\text{all}}$, i.e., first, third, and fifth columns, then $\bar{\boldsymbol{U}}$ will be a 3×3 square matrix.

The eigenfrequency of the system can be obtained by solving the determinant of $\bar{\boldsymbol{U}}$ [20],

$$\Delta = \det \bar{\boldsymbol{U}} = 0 \tag{48}$$

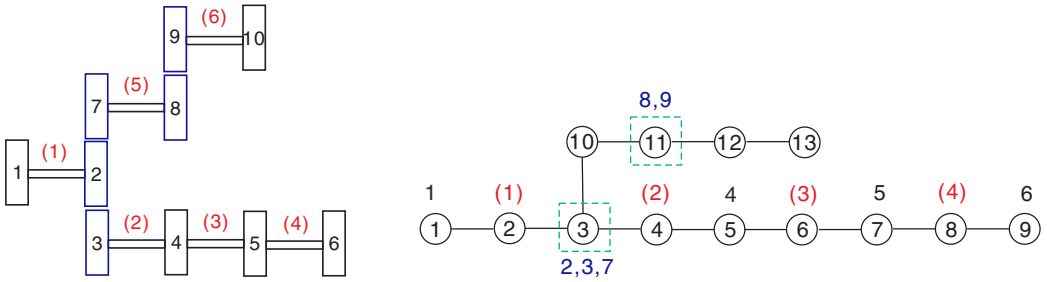

a) A typical tree system with two branches **b) A general topology figure**

Fig. 15 A typical geared branch system in Ref. [11].

Table 2 Moment of inertia and torsional stiffness of each component in the system of Fig. 15a

Disk No.	1	2	3	4	5	6	7	8	9	10
I_i (kg · m^2)	1,098.21	111.45	4.07	45.42	26.44	26.44	0.41	33.90	0.04	9.22
Shaft No.	1	2	3	4	5	6				
k_i (N · m · rad^{-1})	616,897	196,594	3,986,105	7,762,058	219,191	242,917				
Gear ratios	$\frac{N_2}{N_3}$	$\frac{N_2}{N_7}$	$\frac{N_8}{N_9}$							
η	2.3182	4.8182	8.49065							

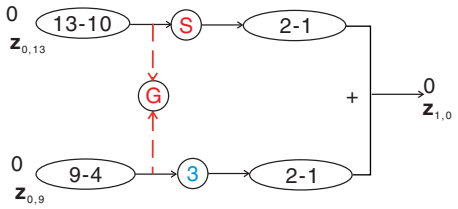

Fig. 16 The topology split into sum of chain systems of Fig. 15b.

Table 3 Frequencies (Hz) of the typical geared branch system in Fig. 15a

Method	Shaft mass[a]	ω_1	ω_2	ω_3	ω_4	ω_5
Present	Considered	23.0870	41.2902	215.2224	376.6524	710.4786
FEM [11]		23.0870	41.2902	215.2224	376.6524	710.4786
Present	Neglected	23.0899	41.3228	217.6013	376.9155	712.6985
FEM [11]		23.0899	41.3228	217.6013	376.9155	712.6985

[a]Mass of the each shaft is considered or neglected.

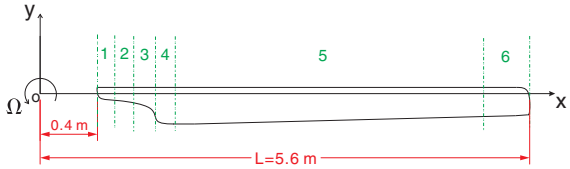

Fig. 17 The rotor blade that divided into six constant cross-section segments.

and the associated eigenvectors can be obtained by adopting the associated eigenfrequency in Eq. (46).

To increase the calculation speed and avoid the leak of roots, zero search for Δ is switched to minimization of the absolute value $|\Delta|$ of the determinant. In fact, any verified optimization strategies like Particle Swarm Optimization (PSO) [33] or Genetic Algorithms (GA) [34] can be applied to this minimization problem. Here, a recursive enumeration-type scanning strategy is adopted that requires only value comparisons [35], i.e.,

$$\Delta := \begin{cases} \Delta & \text{when } |\Delta| \le 1 \\ \text{sign}(\Delta)[1 + \log_{10}|\Delta|] & \text{when } |\Delta| > 1 \end{cases} \tag{49}$$

with frequency range $[1, 3000]$ rad·s^{-1}, 500 grid size, and absolute precision tolerance 1×10^{-9}.

B. Validation

1. *Modeling Method Validation*

To validate the developed method for modeling and analysis of a geared system, the FEM [11] is used to compare the associated results. Firstly, a typical geared branch system given in Ref. [11], which is also presented in Fig. 15, is used for the preliminary validation. The moment of inertia and torsional stiffness of each component are listed in Table 2. Note that the units were converted from imperial units in Ref. [11] to metric units here in Table 2.

The topology figure based on the modeling method proposed here is drawn in Fig. 16, in which the system is represented as two independent chain systems. The explicit expressions for the transfer matrices of the rigid disk, the flexible shaft, the gear, and the virtual

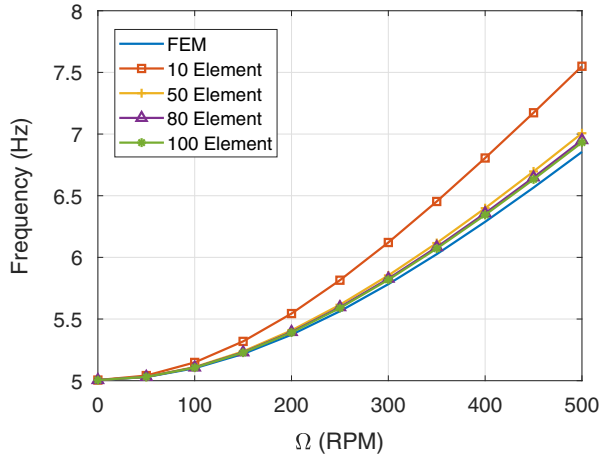

a) The first mode

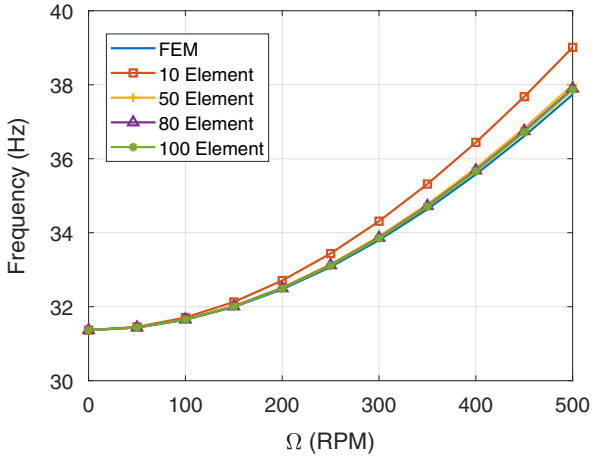

b) The second mode

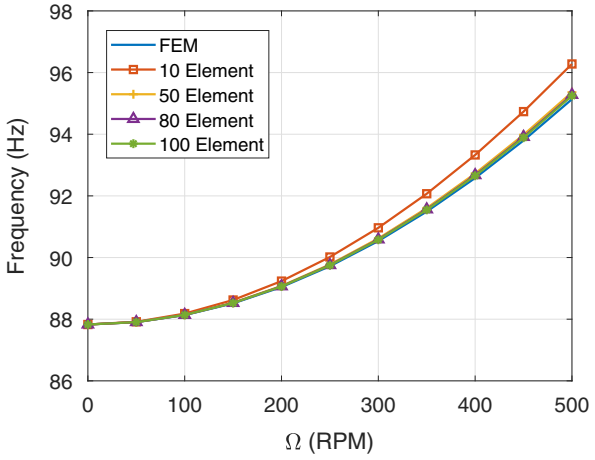

c) The third mode

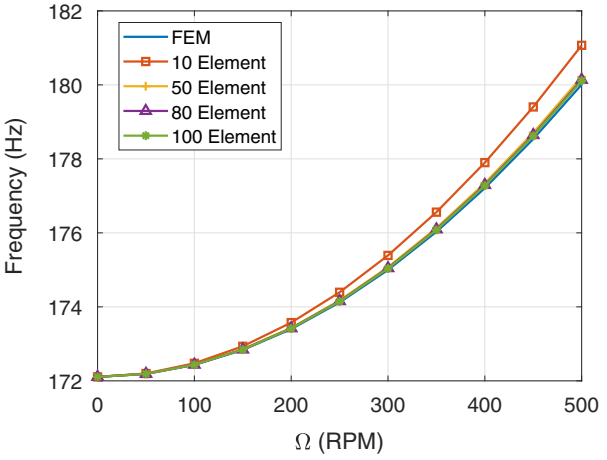

d) The fourth mode

Fig. 18 The frequencies of the first four modes of the hingeless blade.

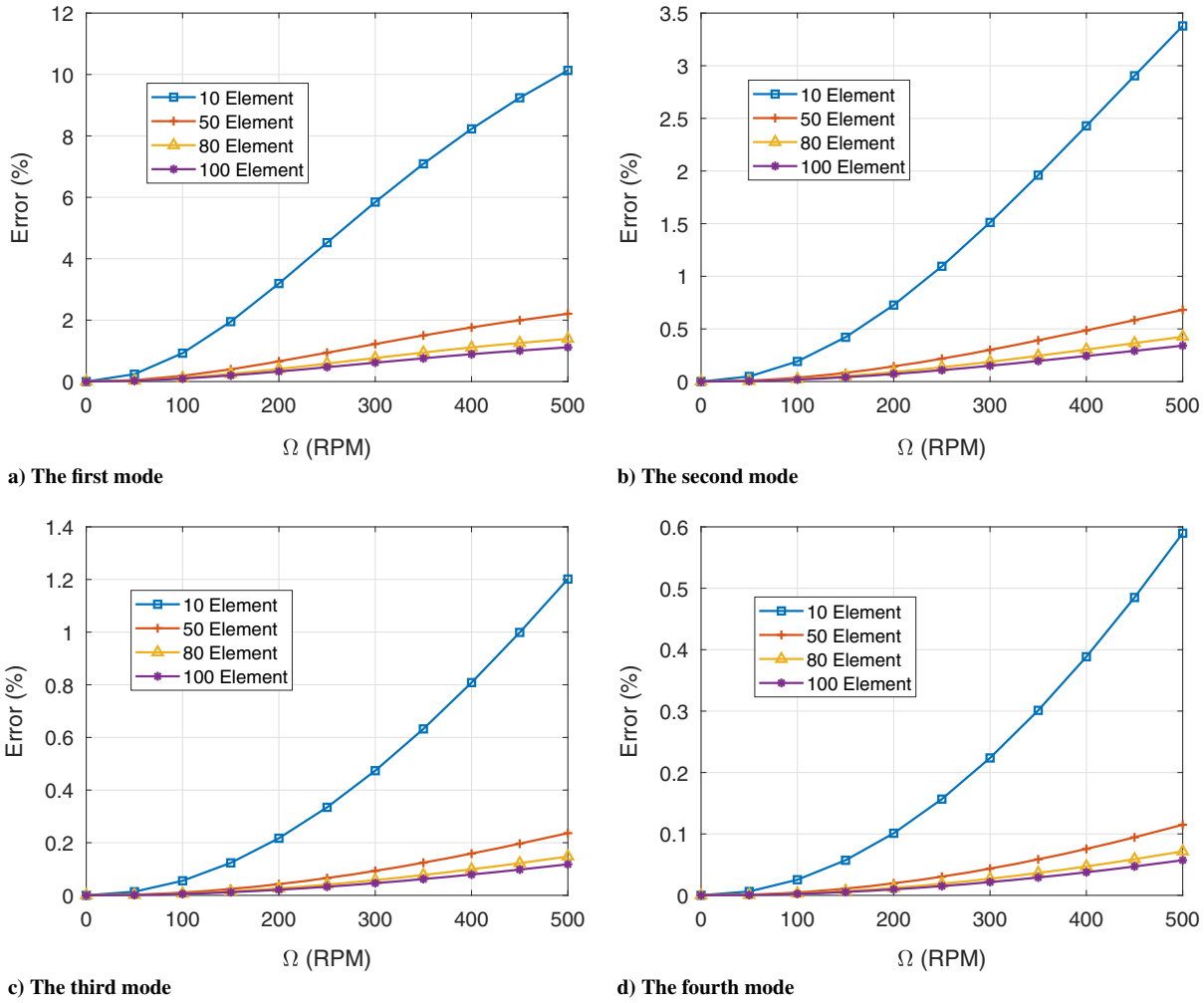

a) The first mode **b) The second mode**

c) The third mode **d) The fourth mode**

Fig. 19 The error of the number of element used, error = |(present − FEM)/FEM| × 100%.

geared branch elements are given in Eqs. (11), (17), (2), and (21), respectively. According to the topology figure of Fig. 16, the equation of motion of the system can be directly written as

$$\begin{bmatrix} \boldsymbol{U}_{13-10}\boldsymbol{U}_F\boldsymbol{U}_{2-1} & \boldsymbol{U}_{9-4}\boldsymbol{U}_3\boldsymbol{U}_{2-1} & -\boldsymbol{I} \\ \boldsymbol{U}_G\boldsymbol{U}_{13-10} & -\boldsymbol{U}_G\boldsymbol{U}_{9-4} & \boldsymbol{0} \end{bmatrix} \begin{Bmatrix} z_{0,13} \\ z_{0,9} \\ z_{1,0} \end{Bmatrix} = \boldsymbol{0} \tag{50}$$

where $\boldsymbol{U}_{j-i}$ is defined as

$$\boldsymbol{U}_{j-i} = \boldsymbol{U}_i\boldsymbol{U}_{i+1} \cdots \boldsymbol{U}_{j-1}\boldsymbol{U}_j \tag{51}$$

Taking the natural boundary condition into the system, the eigenfrequency can be solved and listed in Table 3. Furthermore, the frequency solved by using the FEM is also presented as a comparison. It can be found that the presented method obtained the same results as that of the FEM, no matter whether the mass of the shaft is considered or not.

2. Rotating Beam Element Validation

The calculation accuracy of the developed transfer matrix of the rotating beam is discussed. Specifically, the influence of the number of elements considered in blade modeling is investigated. The schematic of a flexible rotor blade is illustrated in Fig. 17. For the convenience of calculation and presentation here, the blade is discretized into six constant cross-sectional segments as shown in Fig. 17.

The topology of the blade is a typical chain system, and thus the overall transfer matrix of the blade is

$$\boldsymbol{U}_{\text{blade}} = \boldsymbol{U}_1\boldsymbol{U}_2 \cdots \boldsymbol{U}_{n-1}\boldsymbol{U}_n \tag{52}$$

where n is the number of the rotating beam element. Undoubtedly, more elements bring higher accuracy at the cost of more computational resources. The influence of n on calculation accuracy is illustrated in Fig. 18, in which the results obtained by FEM [36] are used as the benchmark. Note that the length of the each element is considered the same here. In Fig. 18, the frequencies of the hingeless blade are plotted as a function of the rotational speed. The associated errors between the present method and the FEM are further illustrated in Fig. 19. It can be found that the maximum error occurs at the first

Table 4 Mass and lead-lag bending stiffness properties of the rotor blade

Segment	1	2	3	4	5	6
x_i (m)	[0.4, 0.7]	[0.7, 0.9]	[0.9, 1.1]	[1.1, 1.6]	[1.6, 5.2]	[5.2, 5.6]
m_0 (kg · m^{-1})	55	40	20	15	10	6
EI (N · m^2)	8×10^6	10×10^6	4×10^6	1.5×10^6	1×10^6	0.6×10^6

Table 5 Frequencies (Hz) of the rotor blade for different rotational speed

Speed, RPM	Rotor	Method	ω_1	ω_2	ω_3	ω_4
0	Articulated	Present	— —	29.9628	96.0766	202.7633
		FEM	— —	29.9632	96.0894	202.8816
	Hingeless	Present	9.3975	55.0981	144.8277	265.2059
		FEM	9.3975	55.0981	144.8277	266.2059
200	Articulated	Present	1.2005	30.9933	96.9638	203.5834
		FEM	1.1777	30.9842	96.9691	203.6946
	Hingeless	Present	9.7252	55.7778	145.4935	266.6422
		FEM	9.7115	55.7637	145.5302	266.9292
350	Articulated	Present	2.1004	33.0143	98.7669	205.2635
		FEM	2.0602	32.9874	98.7571	205.3601
	Hingeless	Present	10.3546	57.1589	146.9566	268.1517
		FEM	10.3160	57.1112	146.9662	268.4132

Table 6 Moment of inertia and torsional stiffness of each component in the drive train system in Fig. 10

Disk No.	1	7	9	11				
I_i (kg · m^2)	10	0.2	0.2	10				
Gear No.	3.1	3.2	5.1	5.2	5.3	5.4	5.5	5.6
I_i (kg · m^2)	0.01	0.01	0.5	0.4	0.4	0.01	0.01	0.01
Shaft No.	2	5	8	11	14			
$\frac{K}{l}$ (N · m^2)	0.15×10^6	0.15×10^6	0.15×10^6	2.0×10^6	6.0×10^6			

mode. The first mode error is about 2%, and the errors of the higher modes do not exceed 1% when 50 elements are adopted. The error steadily increases with the rotational speed Ω, because the assumption that the tension $P(x)$ resulting from the centrifugal force is constant within each beam element is adopted.

Table 7 Gear ratios of the drive train system in Fig. 10

Gear No.	3.1/3.2	5.3/5.2	5.2/5.1	5.4/5.1	5.5/5.1	5.6/5.1
η	1	2.2857	2.5	0.1	0.1	4

The blade whose information is given in Table 4 is utilized for validation. A detailed comparison between the presented method and the FEM [31,37] for both articulated and hingeless blades is given in Table 5. It can be found that the present results have good agreement with that of the FEM for selected rotational speed.

C. Results of the Coupled Blades/Engine/Drive Train System

The blade information of the system as shown in Fig. 10 has been given in Table 4. The moment of inertia and torsional stiffness of each component of the drive train are listed in Table 6. The associated gear ratios are presented in Table 7.

Table 8 Frequencies of the coupled blades/engine/drive train system as shown in Fig. 10 (Hz)

Mode		First	Second[a]	Third	Fourth	Fifth[a]	Sixth
0 RPM	Present	7.9916	9.3975	16.0491	28.7582	55.0981	83.7065
	FEM	7.9916	9.3975	16.0491	28.7582	55.0981	83.7065
350 RPM (nominal rotor speed)	Present	8.2060	10.3546	16.0517	30.6634	57.1589	87.0892
	FEM	8.1883	10.3160	16.0515	31.2118	57.1112	86.0509

[a]Frequency solely related to the rotor blade mode.

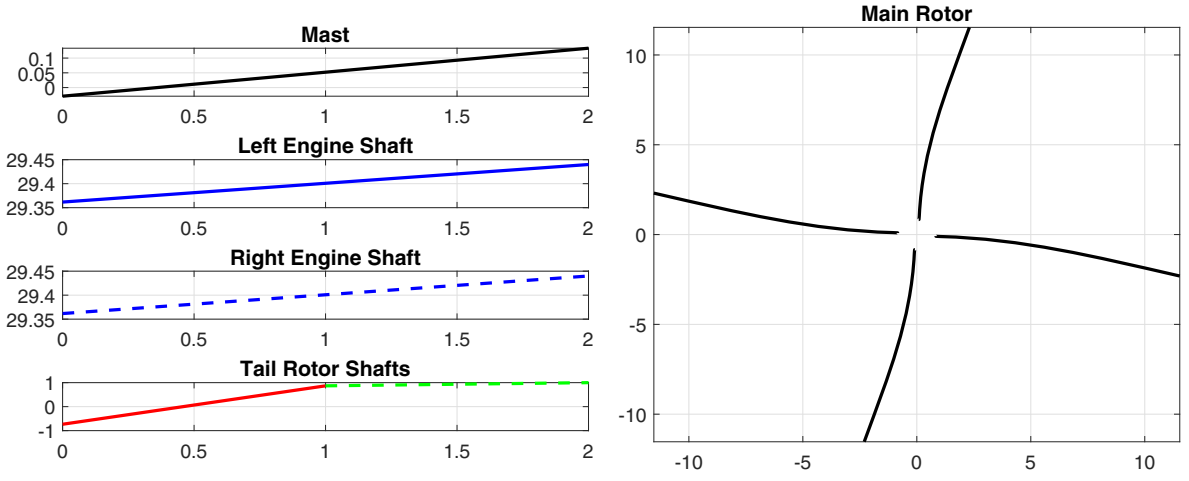

Fig. 20 Mode shape of the first mode.

The frequencies of the coupled helicopter blades/engine/drive train system for selected working conditions are shown in Table 8. Moreover, the results obtained by the FEM are also listed. It can be found that for the nonrotational case, the results obtained by the present method and the FEM are exactly the same. As for the nominal working condition, the results for the two methods also present a great agreement. Actually, the error between these two methods comes from the different approximate strategy for solving the rotating beam. Comparing with the frequency of the isolated hingeless blade as shown in Table 5, it can be found that the second mode and the fifth mode of the coupled system have the same frequency as that of the first mode and the second mode of the blade.

Mode shapes of the first four modes of the coupled system are presented in Figs. 20–23. In these figures, the left sides (0 at the abscissa) of the mast, the engine shafts, and the tail rotor shafts are connected to the main gear box, whereas the right sides (two at the

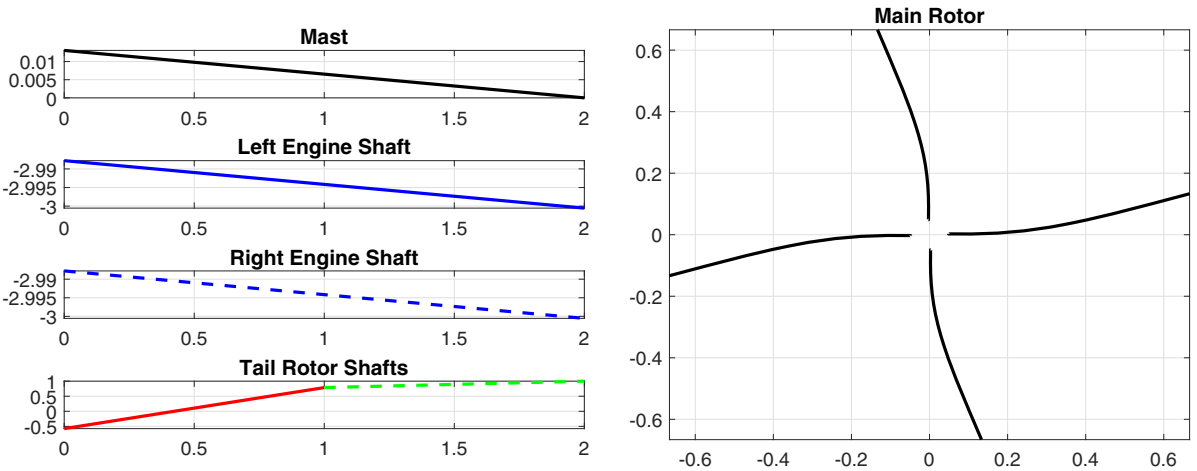

Fig. 21 Mode shape of the second mode.

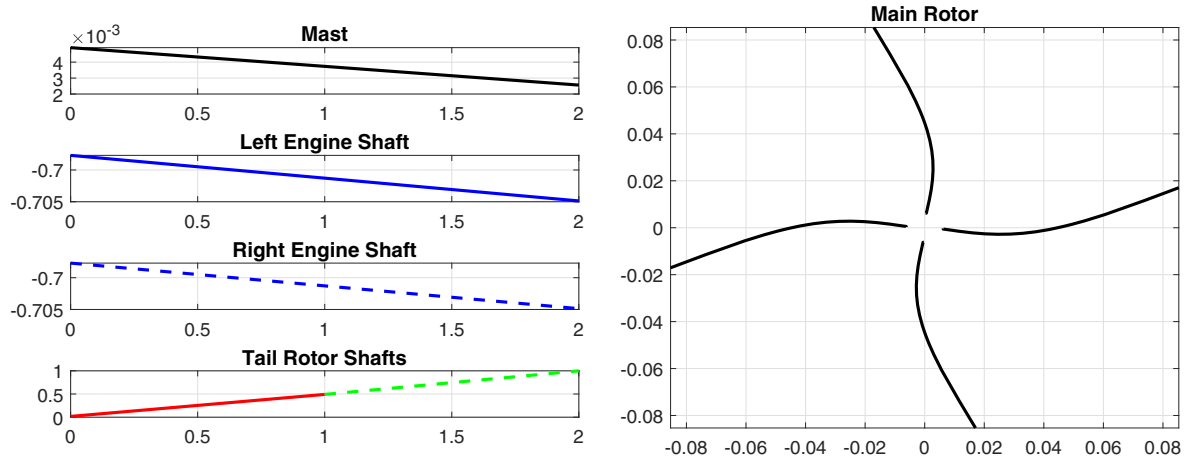

Fig. 22 Mode shape of the third mode.

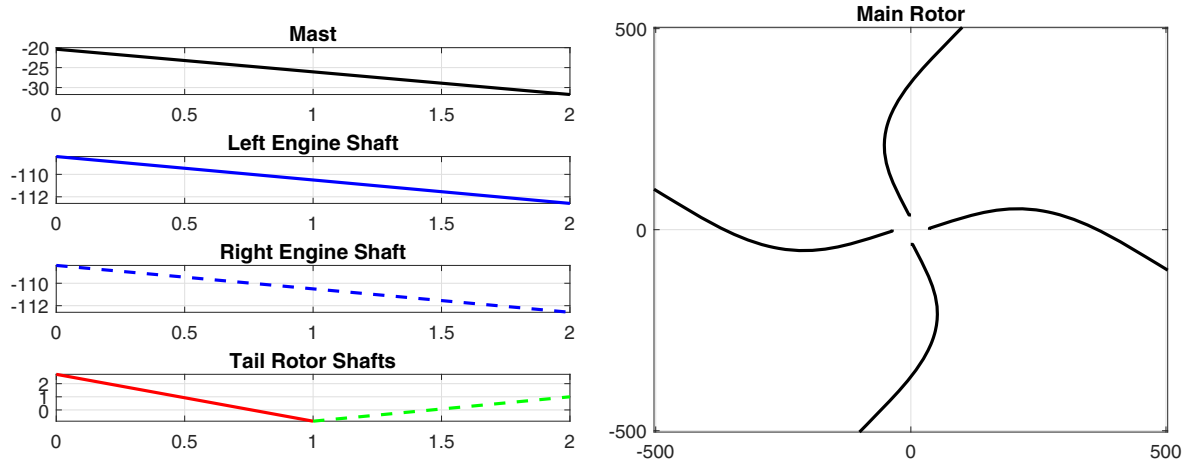

Fig. 23 Mode shape of the fourth mode.

abscissa) of which are connected to the hub, the engines, and the tail rotor, respectively. It can be seen that Figs. 20 and 21 show mode shapes that are essentially identical, only with opposite signs. Moreover, the mode shape of the second mode in Fig. 21 is about 10 times smaller than that of the first mode in Fig. 20, except for the tail rotor shaft rotation. Thus, it seems that the second mode is almost like the first mode, i.e., another collective mode with larger participation of the tail rotor shaft, considering the fact that all blades show identical motion. The second mode of the blade dominates the third and the fourth modes of the coupled system as shown in Figs. 22 and 23. Specifically, a coupled mast and rotor blades mode is the main component of the fourth mode of the system as shown in Fig. 23.

Note that only the collective lead-lag modes are involved in the mode shape of the coupled driven train system, which can be seen in Figs. 20–23. In other words, the drive train is solely coupled with the rotor collective lead-lag modes. Besides, it can be found that the left engine shaft and the right engine shaft have exactly the same mode shapes. Thus, an idea arises from these results to simplify the mathematical modeling of the coupled flexible rotor blade/engine/tail rotor/drive train system, i.e., using one blade element and one engine shaft element to model the multiple rotor blades and the twin engines, respectively. However, this simplification idea is only for identical blades and engines, which means that it would not allow to consider the case of dissimilarities or imperfections.

V. Conclusions

In contrast to creating the equivalent system firstly as that of the FEM, a transfer-matrix-based method is developed to directly obtain the equation of motion of a geared system after defining the transfer matrix of different gear types. A novel modeling strategy is proposed to decouple any geared system topology into a combination of a series of independent chain systems when introducing the virtual geared branch transfer matrix. Thus the governing equation of the system can be written efficiently and conveniently because the transfer matrix method of a chain system is simply matrix multiplication. The developed method will significantly reduce the difficulty of modeling and analysis of the geared system.

In addition, a simpler and more aesthetic transfer matrix of rotating beam is derived to treat both the blade flapping and lead-lag vibration problems. A dimension reduction strategy is also introduced to address the dimension unmatched issue, further reducing the scale of the overall transfer matrix of the system.

An application on modeling and analysis of the coupled flexible rotor blade/engine/tail rotor/drive train system of a helicopter is presented. It can be found that the helicopter drive train is solely coupled with the rotor collective lead-lag modes.

Acknowledgments

The authors thank Foundation of National Key Laboratory of Rotorcraft Aeromechanics (No. 61422202101) and National Natural Science Foundation of China (No. 11802120) for the financial support. Xiao Wang is indebted to Xiaoting Rui of Nanjing University of Science and Technology for his valuable technical advice. The author also expresses his gratitude to Hao Chen and Lingyun Lai of China Helicopter Research and Development Institute of Aviation Industry Corporation of China (AVIC) for their kind assistance. Part of the paper was presented at the 1st International Conference on Mechanical System Dynamics, November 2021, Nanjing, China.

References

[1] Dudley, D. W., *Handbook of Practical Gear Design*, McGraw–Hill, New York, 1984, p. 656.

[2] Johnson, W., *Helicopter Theory*, Princeton Univ. Press, Princeton, NJ, 1980, Chap. 1.

[3] Kuczynski, W., Cooper, D., Twomey, W., and Howlett, J., "The Influence of Engine/Fuel Control Design on Helicopter Dynamics and Handling Qualities," *Journal of the American Helicopter Society*, Vol. 25, No. 2, 1980, pp. 26–34. https://doi.org/10.4050/JAHS.25.26

[4] Hopkins, S. A., Ruzicka, G. C., and Ormiston, R. A., "Analytical Investigations of Coupled Rotorcraft/Engine/Drive Train Dynamics," *Proceedings of the American Helicopter Society: 2nd International Aeromechanics Specialists Conference*, American Helicopter Soc., Oct. 1995, pp. 11–13.

[5] Johnson, W., *Recent Developments in the Dynamics of Advanced Rotor Systems*, NASA Ames Research Center, 1985, Chap. 2.

[6] Guglieri, G., "Effect of Drive Train and Fuel Control Design on Helicopter Handling Qualities," *Journal of the American Helicopter Society*, Vol. 46, No. 1, 2001, pp. 14–22. https://doi.org/10.4050/JAHS.46.14

[7] Muscarello, V., Cocco, L., Favale, M., Masarati, P., and Quaranta, G., "Novel Approach to Interaction Between Engine-Drive Train System and Deformable Rotorcraft Airframes," *73rd International Annual Forum American Helicopter Society (AHS)*, Vertical Flight Soc., Fairfax, VA, May 2017, pp. 1269–1281.

[8] Sidle, S., Sridharan, A., Chopra, I., Feshler, M., and Kull, P., "Investigation of Engine–Airframe Vibration due to Main Rotor Hub Loads Using a Substructuring Framework," *Journal of the American Helicopter Society*, Vol. 64, No. 4, 2019, pp. 1–16. https://doi.org/10.4050/JAHS.64.042001

[9] Rigo, A., Muscarello, V., Masarati, P., Quaranta, G., and Favale, M., "Drive Train Modeling Effects on Tiltrotor Aeroelastic Analysis," *AIAA Scitech 2019 Forum*, AIAA Paper 2019-1367, 2019. https://doi.org/10.2514/6.2019-1367

[10] Weiss, F., and Kessler, C., "Load Prediction of Hingeless Helicopter Rotors Including Drivetrain Dynamics," *CEAS Aeronautical Journal*, Vol. 12, No. 2, 2021, pp. 215–231. https://doi.org/10.1007/s13272-020-00483-6

[11] Wu, J.-S., and Chen, C.-H., "Torsional Vibration Analysis of Gear-Branched Systems by Finite Element Method," *Journal of Sound and Vibration*, Vol. 240, No. 1, 2001, pp. 159–182. https://doi.org/10.1006/jsvi.2000.3197

[12] Kahraman, A., Ozguven, H. N., Houser, D. R., and Zakrajsek, J. J., "Dynamic Analysis of Geared Rotors by Finite Elements," *Journal of Mechanical Design*, Vol. 114, No. 3, 1992, pp. 507–514. https://doi.org/10.1115/1.2926579

[13] Walker, D. N., *Torsional Vibration of Turbo-Machinery*, McGraw–Hill Education, New York, 2004, Chap. 6.

[14] Pestel, E., and Leckie, F. A., *Matrix Methods in Elastomechanics*, McGraw–Hill, New York, 1963, Chap. 1. https://doi.org/10.1016/0020-7403(65)90076-7

[15] Horner, G. C., and Pilkey, W. D., "The Riccati Transfer Matrix Method," *Journal of Mechanical Design*, Vol. 100, No. 2, 1978, pp. 297–302. https://doi.org/10.1115/1.3453915

[16] Uhrig, R., "The Transfer Matrix Method Seen as One Method of Structural Analysis Among Others," *Journal of Sound and Vibration*, Vol. 4, No. 2, 1966, pp. 136–148. https://doi.org/10.1016/0022-460X(66)90117-9

[17] Holzer, H., *Analysis of Torsional Vibration*, Spinger, Berlin, 1921.

[18] Myklestad, N., "New Method of Calculating Natural Modes of Coupled Bending-Torsion Vibration of Beams," *Transactions of ASME*, Vol. 67, No. 1, 1945, pp. 61–67.

[19] Rui, X., Wang, G., Lu, Y., and Yun, L., "Transfer Matrix Method for Linear Multibody System," *Multibody System Dynamics*, Vol. 19, No. 3, 2008, pp. 179–207. https://doi.org/10.1007/s11044-007-9092-0

[20] Rui, X., Wang, G., and Zhang, J., *Transfer Matrix Method for Multibody Systems: Theory and Applications*, Wiley, Hoboken, NJ, 2018, Chap. 1. https://doi.org/10.1002/9781118724811.part2

[21] Rui, X., Zhang, J., and Zhou, Q., "Automatic Deduction Theorem of Overall Transfer Equation of Multibody System," *Advances in Mechanical Engineering*, Vol. 6, Jan. 2014, Paper 378047. https://doi.org/10.1155/2014/378047

[22] Shabana, A. A., "Flexible Multibody Dynamics: Review of Past and Recent Developments," *Multibody System Dynamics*, Vol. 1, No. 2, 1997, pp. 189–222. https://doi.org/10.1023/A:1009773505418

[23] Shabana, A., *Dynamics of Multibody Systems*, Cambridge Univ. Press, London, 2020, Chap. 3. https://doi.org/10.1017/9781108757553

[24] Wittenburg, J., *Dynamics of Multibody Systems*, Springer Science & Business Media, New York, 2007, Chap. 5. https://doi.org/10.1007/978-3-540-73914-2

[25] Abbas, L. K., Zhou, Q., Bestle, D., and Rui, X., "A Unified Approach for Treating Linear Multibody Systems Involving Flexible Beams," *Mechanism and Machine Theory*, Vol. 107, Jan. 2017, pp. 197–209. https://doi.org/10.1016/j.mechmachtheory.2016.09.022

[26] Weiss, F., and Kessler, C., "Drivetrain Influence on the Lead–Lag Modes of Hingeless Helicopter Rotors," *CEAS Aeronautical Journal*, Vol. 11, No. 1, 2020, pp. 67–79. https://doi.org/10.1007/s13272-019-00395-0

[27] Lurie, A. I., *Analytical Mechanics*, Springer Science & Business Media, New York, 2013, Chap. 12. https://doi.org/10.1007/978-3-540-45677-3

[28] Goodno, B. J., and Gere, J. M., *Mechanics of Materials*, 9th ed., Cengage Learning, 2018.

[29] Banerjee, J., Su, H., and Jackson, D., "Free Vibration of Rotating Tapered Beams Using the Dynamic Stiffness Method," *Journal of Sound and Vibration*, Vol. 298, Nos. 4–5, 2006, pp. 1034–1054. https://doi.org/10.1016/j.jsv.2006.06.040

[30] Rui, X., Abbas, L. K., Yang, F., Wang, G., Yu, H., and Wang, Y., "Flapwise Vibration Computations of Coupled Helicopter Rotor/Fuselage: Application of Multibody System Dynamics," *AIAA Journal*, Vol. 56, No. 2, 2018, pp. 818–835. https://doi.org/10.2514/1.J056591

[31] Sivaneri, N. T., and Chopra, I., "Dynamic Stability of a Rotor Blade Using Finite Element Analysis," *AIAA Journal*, Vol. 20, No. 5, 1982, pp. 716–723. https://doi.org/10.2514/3.51129

[32] Dongyang, C., Abbas, L. K., Xiaoting, R., Qing, X., and Marzocca, P., "Dynamic Modeling of Sail Mounted Hydroplanes System-Part I: Modal Characteristics from a Transfer Matrix Method," *Ocean Engineering*, Vol. 130, Jan. 2017, pp. 629–644. https://doi.org/10.1016/j.oceaneng.2016.12.020

[33] Kennedy, J., and Eberhart, R., "Particle Swarm Optimization," *Proceedings of ICNN'95-International Conference on Neural Networks*, Vol. 4, Inst. of Electrical and Electronics Engineers, New York, 1995, pp. 1942–1948. https://doi.org/10.1109/ICNN.1995.488968

[34] Holland, J. H., "Genetic Algorithms," *Scientific American*, Vol. 267, No. 1, 1992, pp. 66–72. https://doi.org/10.1038/scientificamerican0792-66

[35] Bestle, D., Abbas, L., and Rui, X., "Recursive Eigenvalue Search Algorithm for Transfer Matrix Method of Linear Flexible Multibody Systems," *Multibody System Dynamics*, Vol. 32, No. 4, 2014, pp. 429–444. https://doi.org/10.1007/s11044-013-9399-y

[36] Sivaneri, N. T., and Chopra, I., "Finite Element Analysis for Bearingless Rotor Blade Aeroelasticity," *Journal of the American Helicopter Society*, Vol. 29, No. 2, 1984, pp. 42–51. https://doi.org/10.4050/JAHS.29.42

[37] Wang, G., and Wereley, N. M., "Free Vibration Analysis of Rotating Blades with Uniform Tapers," *AIAA Journal*, Vol. 42, No. 12, 2004, pp. 2429–2437. https://doi.org/10.2514/1.4302